뉴노멀시대의 연구:
과학 연구의 새 패러다임

정광열 (Daniel Jeong)

Sales Account Manager
daniel.jeong@jove.com
RMIT University (MSc) 졸업
Swinburne University of Technology
(박사수료, Bioengineering)

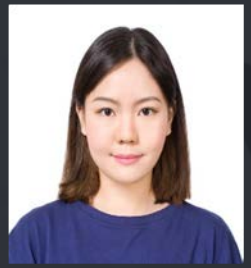

정윤지 (Yunji Jeong)

Product Specialist
yunji.jeong@jove.com
한양대학교 독어독문학과/관광학부 졸업
독일 Bayreuth University International
Business 과정 수료

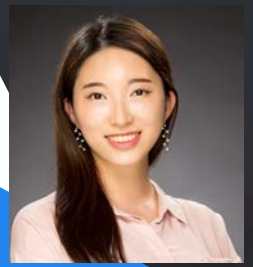

신소라 (Sora Shin)

Product Specialist
sora.shin@jove.com
부산외국어대학교
인도네시아·말레이시아어과
Big Data Utilization Marketing Specialist
과정 수료

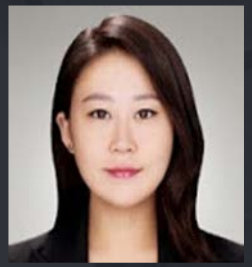

박나은 (NaEun Park)

APAC Marketing Manager
naeun.park@jove.com
Boston University
BSc Mass Communication (PR)
졸업

오승일 (James Oh)

Product Specialist
seungil.oh@jove.com
순천향대학교 의료생명공학과 졸업
순천향대학교 의료과학과 이학석사
(노화, 신경생물학)

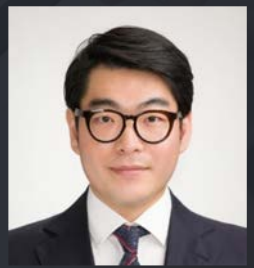

제윤규 (YoonGyu Jae)

Curriculum Specialist
yoongyu.jae@jove.com
경북대학교 생명공학부 졸업
DGIST 대구경북과학기술원 이학박사
(신경과학)

카카오톡 채널 추가하는 방법

jove

2019

2020

How about 2022 ?

2021~

~19

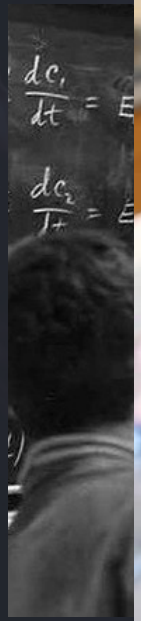

JoVE 소개

Traditional journals: printed on paper

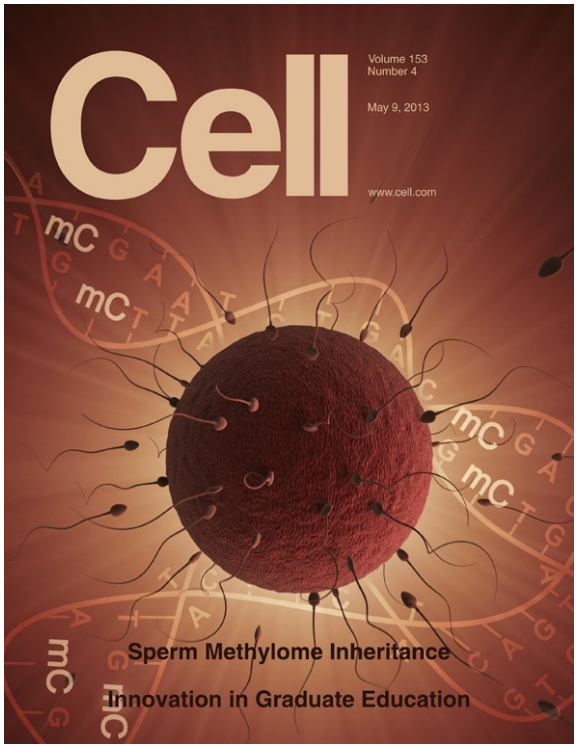

Traditional journals: printed on paper

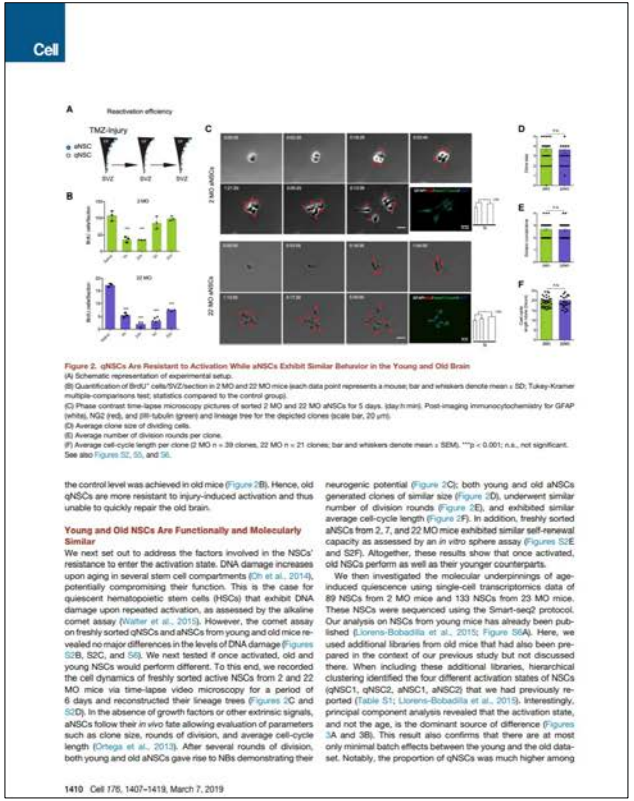

Cell

Figure 2. qNSCs Are Resistant to Activation While aNSCs Exhibit Similar Behavior in the Young and Old Brain

(A) Schematic representation of experimental setup.

(B) Quantification of BrdU+ cells/SVZ/section in 2 MO and 22 MO mice (each data point represents a mouse; bar and whiskers denote mean ± SD; Tukey-Kramer multiple-comparisons test; statistics compared to the control group).

(C) Phase contrast time-lapse microscopy pictures of sorted 2 MO and 22 MO aNSCs for 5 days. (day:h:min). Post-imaging immunocytochemistry for GFAP (white), NG2 (red), and βIII-tubulin (green) and lineage tree for the depicted clones (scale bar, 20 μm).

(D) Average clone size of dividing cells.

(E) Average number of division rounds per clone.

(F) Average cell-cycle length per clone (2 MO n = 39 clones, 22 MO n = 21 clones; bar and whiskers denote mean ± SEM). ***p < 0.001; n.s., not significant.

See also Figures S2, S5, and S6.

the control level was achieved in old mice (Figure 2B). Hence, old qNSCs are more resistant to injury-induced activation and thus unable to quickly repair the old brain.

Young and Old NSCs Are Functionally and Molecularly Similar

We next set out to address the factors involved in the NSCs' resistance to enter the activation state. DNA damage increases upon aging in several stem cell compartments (Oh et al., 2014), potentially compromising their function. This is the case for quiescent hematopoietic stem cells (HSCs) that exhibit DNA damage upon repeated activation, as assessed by the alkaline comet assay (Walter et al., 2015). However, the comet assay on freshly sorted qNSCs and aNSCs from young and old mice revealed no major differences in the levels of DNA damage (Figures S2B, S2C, and S6). We next tested if once activated, old and young NSCs would perform different. To this end, we recorded the cell dynamics of freshly sorted active NSCs from 2 and 22 MO mice via time-lapse video microscopy for a period of 6 days and reconstructed their lineage trees (Figures 2C and S2D). In the absence of growth factors or other extrinsic signals, aNSCs follow their *in vivo* fate allowing evaluation of parameters such as clone size, rounds of division, and average cell-cycle length (Ortega et al., 2013). After several rounds of division, both young and old aNSCs gave rise to NBs demonstrating their neurogenic potential (Figure 2C); both young and old aNSCs generated clones of similar size (Figure 2D), underwent similar number of division rounds (Figure 2E), and exhibited similar average cell-cycle length (Figure 2F). In addition, freshly sorted aNSCs from 2, 7, and 22 MO mice exhibited similar self-renewal capacity as assessed by an *in vitro* sphere assay (Figures S2E and S2F). Altogether, these results show that once activated, old NSCs perform as well as their younger counterparts.

We then investigated the molecular underpinnings of age-induced quiescence using single-cell transcriptomics data of 89 NSCs from 2 MO mice and 133 NSCs from 23 MO mice. These NSCs were sequenced using the Smart-seq2 protocol. Our analysis on NSCs from young mice has already been published (Llorens-Bobadilla et al., 2015; Figure S6A). Here, we used additional libraries from old mice that had also been prepared in the context of our previous study but not discussed there. When including these additional libraries, hierarchical clustering identified the four different activation states of NSCs (qNSC1, qNSC2, aNSC1, aNSC2) that we had previously reported (Table S1; Llorens-Bobadilla et al., 2015). Interestingly, principal component analysis revealed that the activation state, and not the age, is the dominant source of difference (Figures 3A and 3B). This result also confirms that there are at most only minimal batch effects between the young and the old dataset. Notably, the proportion of qNSCs was much higher among

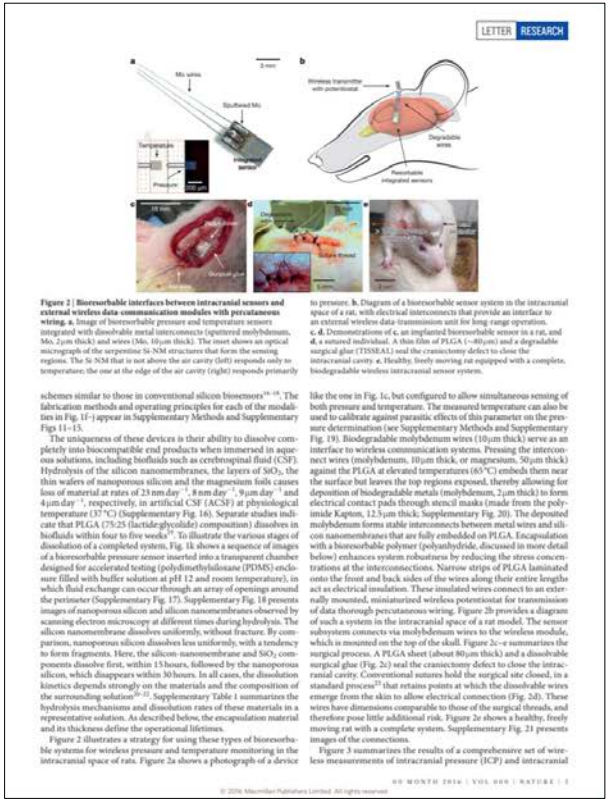

LETTER RESEARCH

Figure 2 | Bioresorbable interfaces between intracranial sensors and external wireless data-communication modules with percutaneous wiring. a, Image of bioresorbable pressure and temperature sensors integrated with dissolvable metal interconnects (sputtered molybdenum, Mo, 2 μm thick) and wires (34o, 10 μm thick). The inset shows an optical micrograph of the serpentine Si-NM structures that form the sensing regions. The Si-NM that is not above the air cavity (left) responds only to temperature; the one at the edge of the air cavity (right) responds primarily to pressure. b, Diagram of a bioresorbable sensor system in the intracranial space of a rat, with electrical interconnects that provide an interface to an external wireless data-transmission unit for long-range operation. c, d, Demonstrations of c, an implanted bioresorbable sensor in a rat, and d, a sutured individual. A thin film of PLGA (~80 μm) and a degradable surgical glue (TISSEAL) seal the craniectomy defect to close the intracranial cavity. e, Healthy, freely moving rat equipped with a complete, biodegradable wireless intracranial sensor system.

schemes similar to those in conventional silicon biosensors[16–18]. The fabrication methods and operating principles for each of the modalities in Fig. 1f–j appear in Supplementary Methods and Supplementary Figs 11–15.

The uniqueness of these devices is their ability to dissolve completely into biocompatible end products when immersed in aqueous solutions, including biofluids such as cerebrospinal fluid (CSF). Hydrolysis of the silicon nanomembranes, the layers of SiO_2, the thin wafers of nanoporous silicon and the magnesium foils causes loss of material at rates of 23 nm day^{-1}, 8 nm day^{-1}, 9 μm day^{-1} and 4 μm day^{-1}, respectively, in artificial CSF (ACSF) at physiological temperature (37 °C) (Supplementary Fig. 16). Separate studies indicate that PLGA (75:25 (lactide:glycolide) composition) dissolves in biofluids within four to five weeks[19]. To illustrate the various stages of dissolution of a completed system, Fig. 1k shows a sequence of images of a bioresorbable pressure sensor inserted into a transparent chamber designed for accelerated testing (polydimethylsiloxane (PDMS) enclosure filled with buffer solution at pH 12 and room temperature), in which fluid exchange can occur through an array of openings around the perimeter (Supplementary Fig. 17). Supplementary Fig. 18 presents images of nanoporous silicon and silicon nanomembranes observed by scanning electron microscopy at different times during hydrolysis. The silicon nanomembrane dissolves uniformly, without fracture. By comparison, nanoporous silicon dissolves less uniformly, with a tendency to form fragments. Here, the silicon–nanomembrane and SiO_2 components dissolve first, within 15 hours, followed by the nanoporous silicon, which disappears within 30 hours. In all cases, the dissolution kinetics depends strongly on the materials and the composition of the surrounding solution[20–22]. Supplementary Table 1 summarizes the hydrolysis mechanisms and dissolution rates of these materials in a representative solution. As described below, the encapsulation material and its thickness define the operational lifetimes.

Figure 2 illustrates a strategy for using these types of bioresorbable systems for wireless pressure and temperature monitoring in the intracranial space of rats. Figure 2a shows a photograph of a device like the one in Fig. 1c, but configured to allow simultaneous sensing of both pressure and temperature. The measured temperature can also be used to calibrate against parasitic effects of this parameter on the pressure determination (see Supplementary Methods and Supplementary Fig. 19). Biodegradable molybdenum wires (10 μm thick) serve as an interface to wireless communication systems. Pressing the interconnect wires (molybdenum, 10 μm thick, or magnesium, 50 μm thick) against the PLGA at elevated temperatures (65 °C) embeds them near the surface but leaves the top regions exposed, thereby allowing for deposition of biodegradable metals (molybdenum, 2 μm thick) to form electrical contact pads through stencil masks (made from the polyimide Kapton, 12.5 μm thick; Supplementary Fig. 20). The deposited molybdenum forms stable interconnects between metal wires and silicon nanomembranes that are fully embedded on PLGA. Encapsulation with a bioresorbable polymer (polyanhydride, discussed in more detail below) enhances system robustness by reducing the stress concentrations at the interconnections. Narrow strips of PLGA laminated onto the front and back sides of the wires along their entire lengths act as electrical insulation. These insulated wires connect to an externally mounted, miniaturized wireless potentiostat for transmission of data thorough percutaneous wiring. Figure 2b provides a diagram of such a system in the intracranial space of a rat model. The sensor subsystem connects via molybdenum wires to the wireless module, which is mounted on the top of the skull. Figure 2c–e summarizes the surgical process. A PLGA sheet (about 80 μm thick) and a dissolvable surgical glue (Fig. 2c) seal the craniectomy defect to close the intracranial cavity. Conventional sutures hold the surgical site closed, in a standard process[23] that retains points at which the dissolvable wires emerge from the skin to allow electrical connection (Fig. 2d). These wires have dimensions comparable to those of the surgical threads, and therefore pose little additional risk. Figure 2e shows a healthy, freely moving rat with a complete system. Supplementary Fig. 21 presents images of the connections.

Figure 3 summarizes the results of a comprehensive set of wireless measurements of intracranial pressure (ICP) and intracranial

© 2016 Macmillan Publishers Limited. All rights reserved.

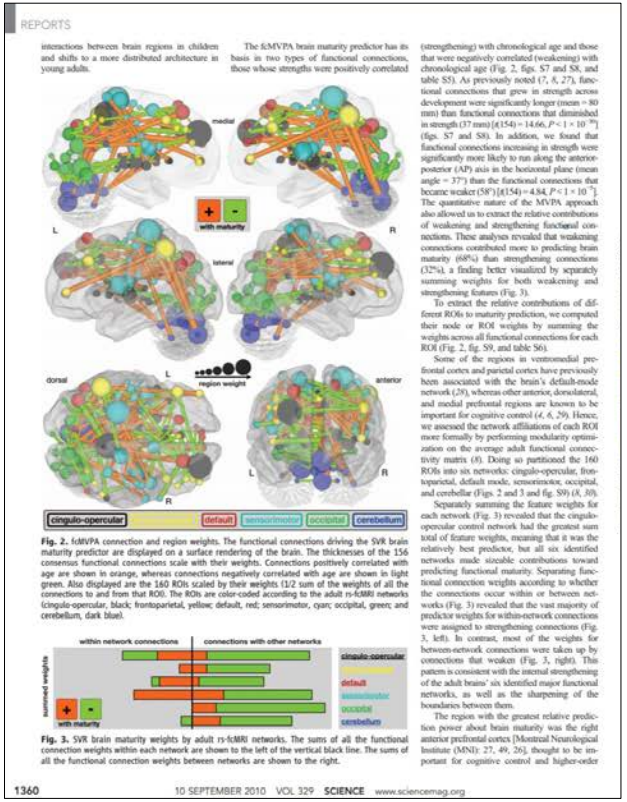

REPORTS

interactions between brain regions in children and shifts to a more distributed architecture in young adults.

The fcMVPA brain maturity predictor has its basis in two types of functional connections, those whose strengths were positively correlated (strengthening) with chronological age and those that were negatively correlated (weakening) with chronological age (Fig. 2, figs. S7 and S8, and table S5). As previously noted (7, 8, 27), functional connections that grew in strength across development were significantly longer (mean = 80 mm) than functional connections that diminished in strength (37 mm) ($t(154) = 14.66$, $P < 1 \times 10^{-30}$) (figs. S7 and S8). In addition, we found that functional connections increasing in strength were significantly more likely to run along the anterior-posterior (AP) axis in the horizontal plane (mean angle = 37°) than the functional connections that became weaker (58°) ($t(154) = 4.84$, $P < 1 \times 10^{-5}$). The quantitative nature of the MVPA approach also allowed us to extract the relative contributions of weakening and strengthening functional connections. These analyses revealed that weakening connections contributed more to predicting brain maturity (68%) than strengthening connections (32%), a finding better visualized by separately summing weights for both weakening and strengthening features (Fig. 3).

To extract the relative contributions of different ROIs to maturity prediction, we computed their node or ROI weights by summing the weights across all functional connections for each ROI (Fig. 2, fig. S9, and table S6).

Some of the regions in ventromedial prefrontal cortex and parietal cortex have previously been associated with the brain's default-mode network (28), whereas other anterior, dorsolateral, and medial prefrontal regions are known to be important for cognitive control (4, 6, 29). Hence, we assessed the network affiliations of each ROI more formally by performing modularity optimization on the average adult functional connectivity matrix (8). Doing so partitioned the 160 ROIs into six networks: cingulo-opercular, frontoparietal, default mode, sensorimotor, occipital, and cerebellar (Figs. 2 and 3 and fig. S9) (8, 30).

Separately summing the feature weights for each network (Fig. 3) revealed that the cingulo-opercular control network had the greatest sum total of feature weights, meaning that it was the relatively best predictor, but all six identified networks made sizeable contributions toward predicting functional maturity. Separating functional connection weights according to whether the connections occur within or between networks (Fig. 3, right). This pattern is consistent with the internal strengthening of the adult brains' six identified major functional networks, as well as the sharpening of the boundaries between them.

The region with the greatest relative prediction power about brain maturity was the right anterior prefrontal cortex [Montreal Neurological Institute (MNI): 27, 49, 26], thought to be important for cognitive control and higher-order

Fig. 2. fcMVPA connection and region weights. The functional connections driving the SVR brain maturity predictor are displayed on a surface rendering of the brain. The thicknesses of the 156 consensus functional connections scale with their weights. Connections positively correlated with age are shown in orange, whereas connections negatively correlated with age are shown in light green. Also displayed are the 160 ROIs scaled by their weights (1/2 sum of the weights of all the connections to and from that ROI). The ROIs are color-coded according to the adult rs-fcMRI networks (cingulo-opercular, black; frontoparietal, yellow; default, red; sensorimotor, cyan; occipital, green; and cerebellum, dark blue).

Fig. 3. SVR brain maturity weights by adult rs-fcMRI networks. The sums of all the functional connection weights within each network are shown to the left of the vertical black line. The sums of all the functional connection weights between networks are shown to the right.

JoVE: Better understanding for Scientists

TEXT ARTICLE

"Once sodium azide has evaporated, line up animals to desired imaging setup. Move the animals side by side with anterior and posterior sides in the same orientation for all animals. Image animals immediately..."

REAL LIFE

Reading < Visualizing

jove

- Journal of Visualized Experiments

- 세계 최초 Peer Reviewed 비디오 저널 (IF 1.2)

- 다양한 분야의 각종 실험 및 연구방법, 교육내용을 비디오 / PDF 형식으로 제공

- 동영상으로 녹화한 실험 및 연구방법을 활용해 연구 시간 단축 및 연구 비용 절약에 도움

- 동영상 컨텐츠는 수업/교육 시 활용 가능


jove
JoVE Research

About JoVE Research

jove

RESEARCH

JoVE Research는 여러 분야의 과학적 연구를 보여주는 비디오 라이브러리로 과학 연구를 더욱더 발전시키고 실험실에서의 생산성을 높이기위해 만들어진 솔루션입니다.

최첨단 실험, 필수 기술 및 표준 프로토콜에 대한 비디오 데모를 통해 JoVE Research는 전 세계 기관이 연구 목표를 달성하도록 지원합니다.

10,000+ 연구 영상

1,200+ 새로운 비디오 기사

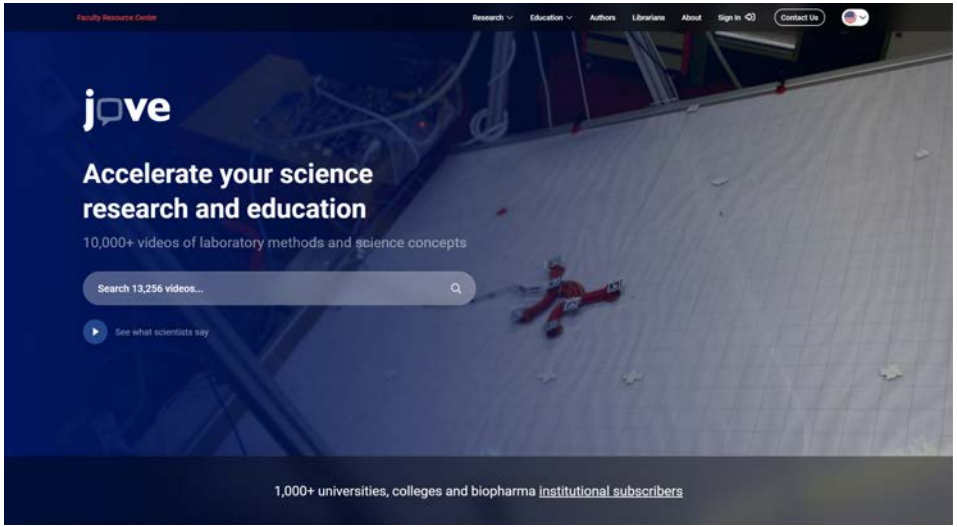

Features of JoVE Research

연구 생산성/재현성 향상 | 시간/재료비 절약 | 연구 효율 증진

Productivity & Reproducibility

다른 실험실에서 우리가 JoVE에 출판한
동일한 결과를 얻을 수 있도록 도와줍니다.

- Marilene Pavan, Boston University

Time & Resources

기회 비용의 절약
(연간 재료비 20%, 인건비 $5700, 연구 시간 2336 h)

–Valerie Rezek, UCLA

On Boarding & Training

JoVE 영상을 통해 새로운 연구자들은 며칠
안에 방법을 쉽게 익힐 수 있습니다.

- Fairbanks Jeanette Moore, University of Alaska

Publication

- 학생들에게 표준화 된 교육 제공 후속
- 연구들을 더욱더 빠르게 진행

- Clemson University Dr. Delphine Dean

JoVE 활용 사례

JoVE의 활용 사례 1 (실험 수행)

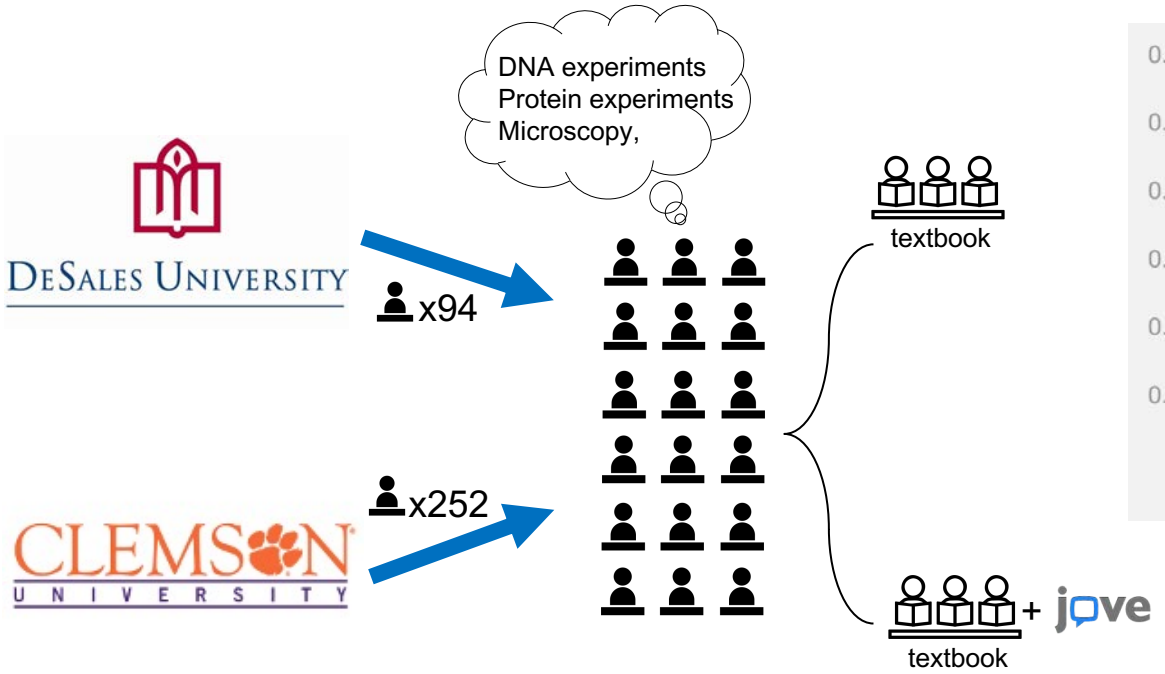

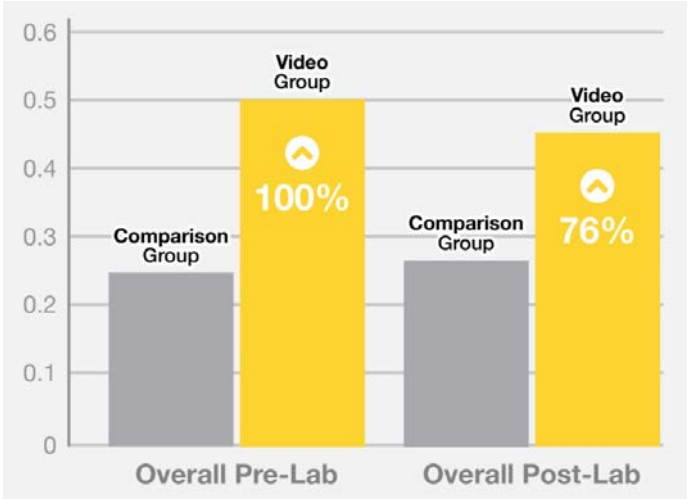

JoVE를 활용한 그룹이 실험 전/후에
더 높은 이해도/수행

JoVE의 활용 사례 2 (수업 이해)

x500

수업 | 수업 + jove

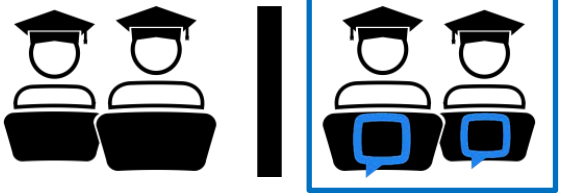

<일반 화학 수업 진행>

엔탈피, 엔트로피, 반응 속도,
르샤틀리에 원리 etc.

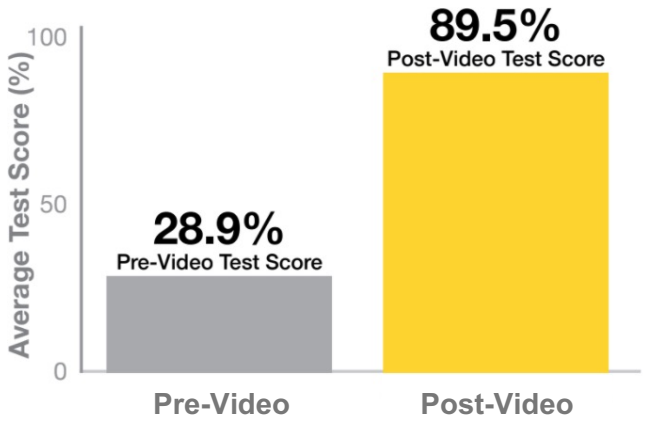

수업 후 JoVE를 활용한 그룹이 시험 점수에서 향상된 결과를 나타냄을 입증

JoVE의 활용 사례 3 (연구 효율)

Dr. Theresa Casey (Assis. Prof., Purdue Univ.)

"저는 20년 동안 연구를 해왔는데,
jove 를 이용하고 난 이후로 연구가 훨씬
쉬워졌습니다. 타 연구자들이 수행하는 연구 내용을
배우고, 실험 전 필수 기술을 익힐 수 있기 때문입니다."

jove 활용 배경

- ▶ 시교차 상핵 수술 (suprachiasmatic nucleus surgery) 교육 필요
- ▶ 다른 나라의 연구실을 방문하는 현장 교육을 받기 위해 시간적, 경제적 투자 발생 직면
- ▶ 배워야 하는 프로토콜을 정확하고 상세하게 보여주는 jove 비디오 저널을 찾게 됨

jove 활용 이점

시간 효율
총 연구 소요 기간이
약 2달에서 2주로 줄어듦

시행착오 완화
시행착오 감소로 인한
시약 비용 $7,700 절감

비용 절감
교육 효율성 증대로
$6,300 인건비 및 $1,100
출장 비용 감소

JoVE의 활용 사례 4 (교육 효율)

Dr. Anna Kirby, M.D.
(Royal Marsden NHS Foundation Trust)

“ jove 덕분에 저희가 직접 교육을 하러 출장을 가지 않아도, 온라인으로 프로토콜을 더 정확히 전달할 수 있기 때문에, 많은 시간이 절약되었습니다.”

jove 활용 배경

- ▶ 수많은 의료진들이 특정 기법* 트레이닝을 요청하였으나, 짧은 시간 내에 모든 인원을 교육해야 하는 어려움 직면
- ▶ 프로토콜을 jove 에 출간하여 전 세계 의료진에게 비디오와 텍스트 형태로 단계별 상세 설명 가능

jove 활용 이점

시간 효율
36개국 전세계 의료진이 단시간 내 프로토콜 습득

높은 만족도
10명 중 9명의 의료진이 비디오가 충분한 자료가 된다는 응답 확인

원활한 활용도
해당 비디오 조회수 36,000회 도달 및 41개 과학 출판물 인용

* 유방암 환자들의 방사선 치료 중 심장 부위를 방사능으로부터 보호 하는 기술

JoVE에 논문 게재하는 방법

Publication Process

You've already done all the hard work, we'll do the rest...

MANUSCRIPT SUBMISSION

Authors submit a traditional text manuscript, including a step-by-step protocol and representative results.

PEER-REVIEW & SCRIPTING

If accepted, the manuscript is turned into a script by our PhD-level script writers.

PRODUCTION

A videographer films at your lab for one day. We edit the footage and add a professional voiceover.

PUBLICATION

The article is published on JoVE and indexed in Web of Science and PubMed.

jove

JoVE Journal submission

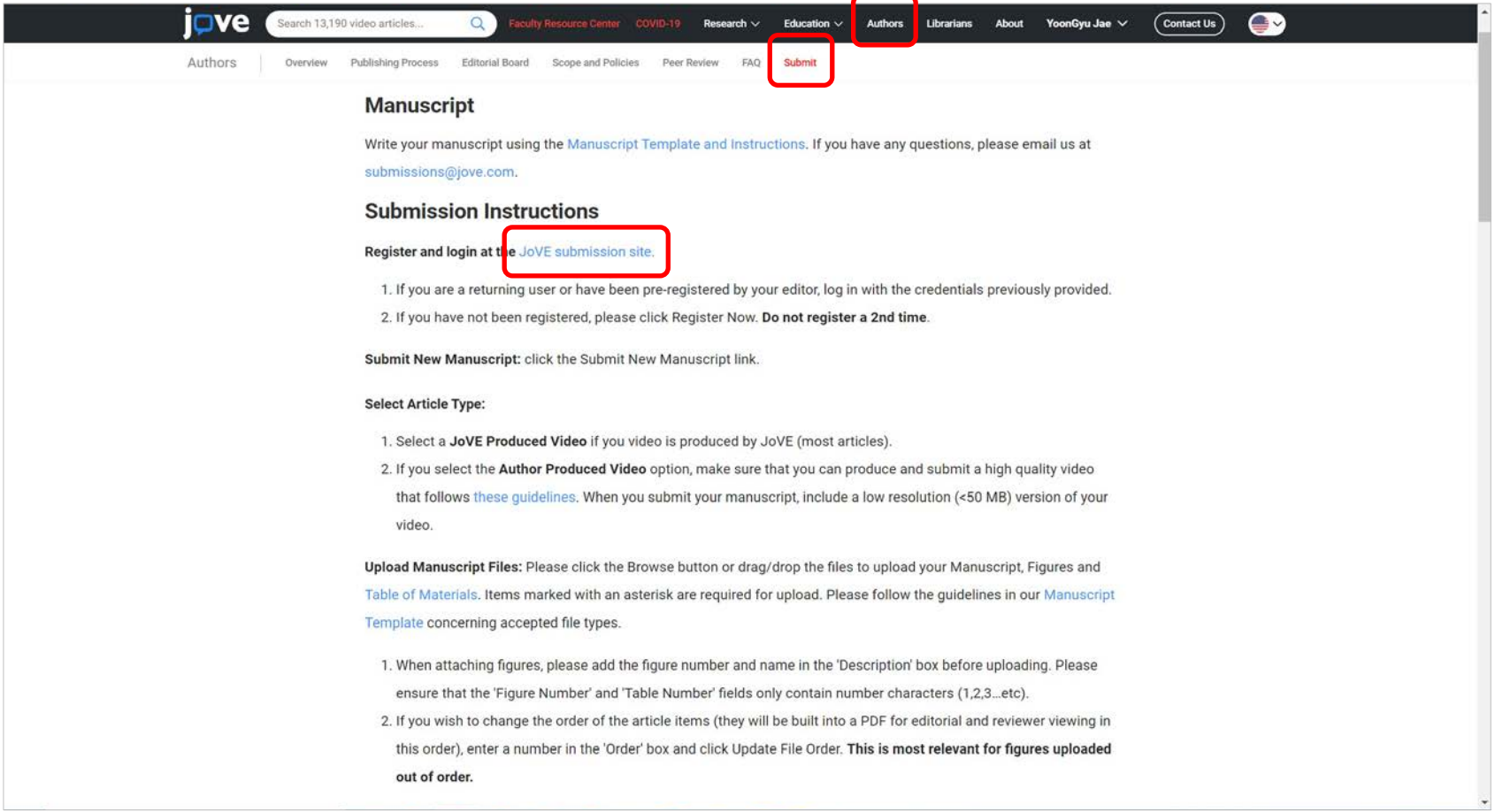


[Music]


jove
코로나 시대의
연구 트렌드 변화

새로운 연구 주제/공유 방식 등장과 연구 가속화

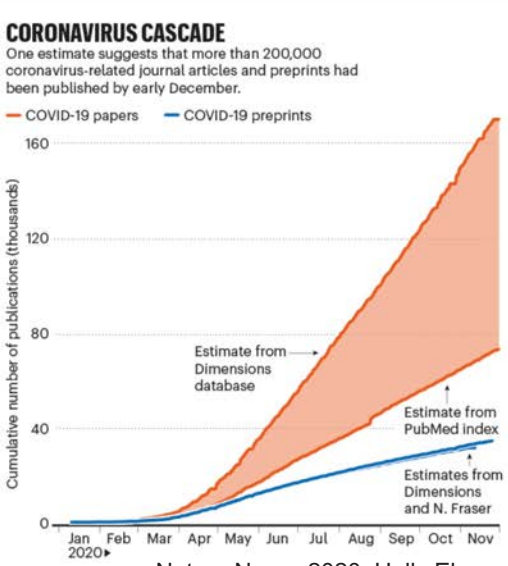

Nature News, 2020, Holly Else

새로운 연구 주제
: Covid-19 논문의 증가

itu.int

대학 교육 / 학술 미팅 방식 변화
: 웨비나의 등장과 활성화

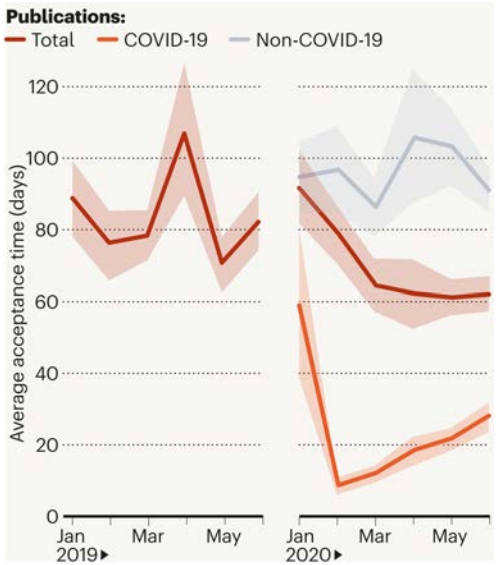

Nature News, 2020, Holly Else

Covid-19 논문 발행 속도 가속화

코로나 일상화에 의한 과학/기술 주제의 다양화

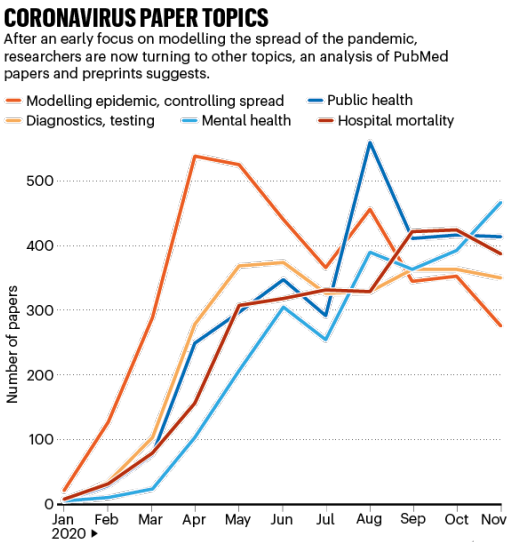

Nature News, 2020, Holly Else

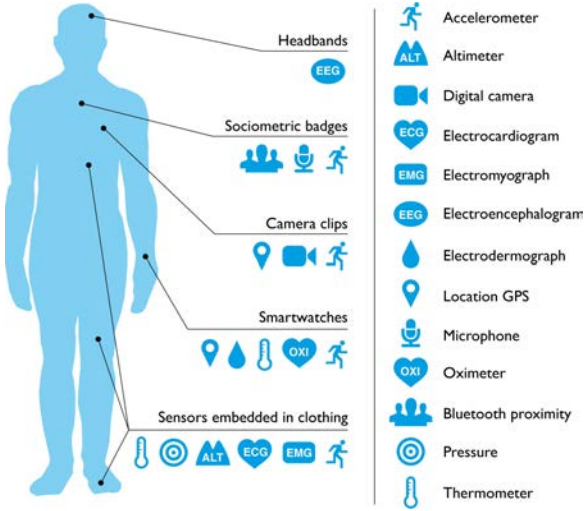

Rise of Consumer Health Wearables: Promises and Barriers., Plos Med.

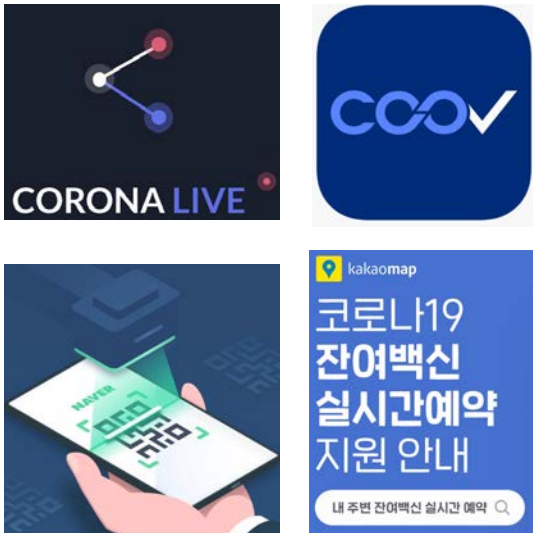

코로나 장기화 → 연구 주제의 다양화

Wearable Health tracking device의 발전과 보급

코로나 관련 앱/프로그램 활성화 통신-빅데이터 기반

초청 연사와 함께하는 포스트 펜데믹 시대의 과학 연구

정예지 박사

- 오하이오 주립대 수의과 대학 병리과 레지던트
- 존스홉킨스 대학교 의과대학 박사

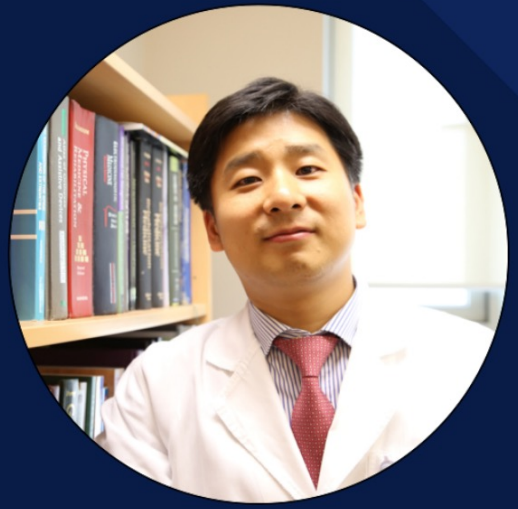

김원석 교수

- 분당서울대학교병원 재활의학과 부교수
- 서울대학교 의과대학 재활의학과 박사

카카오톡 채널 추가하는 방법

jove

Questions?


Thanks for Listening
Curriculum Specialist 제윤규 Ph.D.
yoongyu.jae@jove.com
/jove
@JoVEJournal
/jovejournal
/JOVEjournal
Jove Korea